METABOLISM

The kinase PKD3 provides negative feedback on cholesterol and triglyceride synthesis by suppressing insulin signaling

Alexander E. Mayer[1], Mona C. Löffler[1], Angel E. Loza Valdés[1], Werner Schmitz[2], Rabih El-Merahbi[1], Jonathan Trujillo Viera[1], Manuela Erk[1], Thianzhou Zhang[3]*, Ursula Braun[3†], Mathias Heikenwalder[4], Michael Leitges[3‡], Almut Schulze[2], Grzegorz Sumara[1,5§]

Hepatic activation of protein kinase C (PKC) isoforms by diacylglycerol (DAG) promotes insulin resistance and contributes to the development of type 2 diabetes (T2D). The closely related protein kinase D (PKD) isoforms act as effectors for DAG and PKC. Here, we showed that PKD3 was the predominant PKD isoform expressed in hepatocytes and was activated by lipid overload. PKD3 suppressed the activity of downstream insulin effectors including the kinase AKT and mechanistic target of rapamycin complex 1 and 2 (mTORC1 and mTORC2). Hepatic deletion of PKD3 in mice improved insulin-induced glucose tolerance. However, increased insulin signaling in the absence of PKD3 promoted lipogenesis mediated by SREBP (sterol regulatory element-binding protein) and consequently increased triglyceride and cholesterol content in the livers of PKD3-deficient mice fed a high-fat diet. Conversely, hepatic-specific overexpression of a constitutively active PKD3 mutant suppressed insulin-induced signaling and caused insulin resistance. Our results indicate that PKD3 provides feedback on hepatic lipid production and suppresses insulin signaling. Therefore, manipulation of PKD3 activity could be used to decrease hepatic lipid content or improve hepatic insulin sensitivity.

INTRODUCTION

Hepatocytes are a major target for insulin. On the one hand, insulin stimulates hepatic glucose uptake, suppresses de novo glucose production, and, therefore, lowers systemic glycemia (*1*). On the other hand, excessive insulin signaling promotes de novo lipid synthesis and, consequently, the accumulation of triglycerides (TGs) and cholesterol in hepatocytes. This can lead to the development of nonalcoholic fatty liver disease (NAFLD), hepatic insulin resistance, and eventually to the development of nonalcoholic steatohepatitis (NASH) and, consequently, to liver cirrhosis (*2*). On the molecular level, insulin stimulates activity and expression of major transcription factors such as sterol regulatory binding proteins (SREBPs) that promote hepatic lipid production (*3*). Activation of SREBP-dependent transcription requires inputs from various insulin-evoked signaling cascades, which include AKT and mechanistic target of rapamycin complex 1 and 2 (mTORC1 and mTORC2) (*3*, *4*).

Obesity-related metabolic overload results in the accumulation of diacylglycerol (DAG) in the liver (*5*). Protein kinase C (PKC) isoforms mediate DAG-evoked insulin resistance (*2*, *5*). The major PKC isoform expressed in the liver, PKCε, promotes insulin resistance by phosphorylating the insulin receptor to inhibit downstream signaling (*6*, *7*). Protein kinase D (PKD) isoforms (PKD1, PKD2, and PKD3) are DAG and PKC effectors that integrate multiple nutritional and hormonal inputs (*8*). However, the impact of PKDs on hepatic metabolism has not been investigated so far. Different PKDs have been implicated in the regulation of muscle differentiation, function of adipose tissue, pathophysiological heart remodeling, immune response, carcinogenesis, blood coagulation, insulin secretion, actin remodeling, trans-Golgi network dynamics, cell proliferation, and migration (*8*–*20*).

Here, we showed that PKD3 was the predominant PKD isoform in the liver and was activated in lipid-loaded hepatocytes. Furthermore, we demonstrated that PKD3 suppressed insulin signaling, resulting in impaired AKT phosphorylation and activation of mTORC1 and mTORC2. Mice lacking PKD3 in hepatocytes presented improved glucose and insulin tolerance and elevated SREBP-dependent lipogenesis, which resulted in increased hepatic TG and cholesterol content. These results indicate that PKD3 attenuates insulin signaling, thereby preventing the development of fatty liver.

RESULTS

Lipid accumulation promotes PKD3 activation in the liver

Hepatic DAG accumulation in the liver has been postulated to contribute to insulin resistance in obese subjects (*5*). We found that mice fed a high-fat diet (HFD) accumulated significantly more DAG species compared to normal diet (ND)–fed mice in the liver (Fig. 1A). PKD isoforms are activated in response to stimulation of receptors that use DAG as a secondary messenger (*8*). We observed that stimulation of isolated primary hepatocytes with a cell-permeable analog of DAG (1,2-dioctanoyl-*sn*-glycerol) resulted in PKD activation as indicated by the phosphorylation of two serine residues in the activating loop in the kinase domain (Fig. 1B and fig. S1A). Moreover, long-term incubation of hepatocytes with oleic acid, which induces DAG and TG accumulation in cells, also led to PKD activation (Fig. 1C and fig. S1B). Although DAG accumulates during obesity, our data suggest that DAG-evoked signaling might provide negative feedback

[1]Rudolf Virchow Center for Experimental Biomedicine, University of Würzburg, 97080 Würzburg, Germany. [2]Theodor Boveri Institute, Biocenter, University of Würzburg, 97074 Würzburg, Germany. [3]Biotechnology Centre of Oslo, University of Oslo, 0349 Oslo, Norway. [4]Division of Chronic Inflammation and Cancer, German Cancer Research Center (DKFZ), 69120 Heidelberg, Germany. [5]Nencki Institute of Experimental Biology, PAS, 02-093 Warsaw, Poland.
*Present address: Li Ka Shing Knowledge Institute (LKSKI), St. Michael's Hospital, M5B 1W8 Toronto, Canada.
†Present address: National Core Facility for Human Pluripotent Stem Cells, Oslo University Hospital, 0372 Oslo, Norway.
‡Present address: Tier 1 Canada Research Chair in Cell Signalling and Translational Medicine, Memorial University of Newfoundland, A1B 3V6 St. John's, Canada.
§Corresponding author. Email: grzegorz.sumara@uni-wuerzburg.de

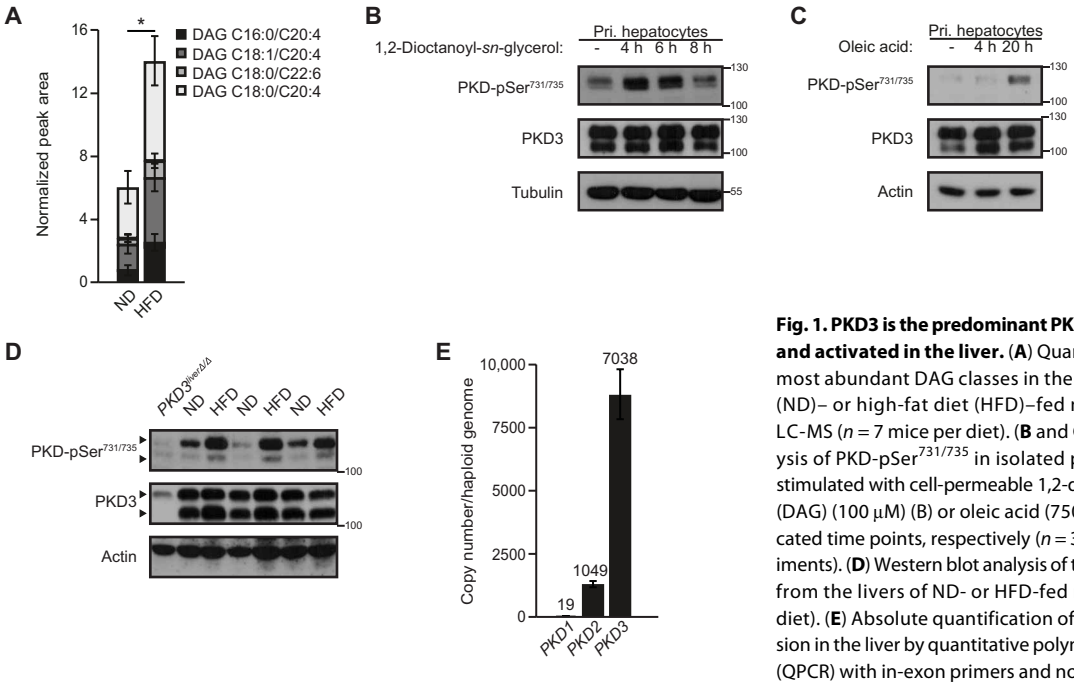

Fig. 1. PKD3 is the predominant PKD isoform expressed and activated in the liver. (**A**) Quantification of the four most abundant DAG classes in the livers of normal diet (ND)– or high-fat diet (HFD)–fed mice determined by LC-MS ($n = 7$ mice per diet). (**B** and **C**) Western blot analysis of PKD-pSer$^{731/735}$ in isolated primary hepatocytes stimulated with cell-permeable 1,2-dioctanoyl-*sn*-glycerol (DAG) (100 μM) (B) or oleic acid (750 μM) (C) for the indicated time points, respectively ($n = 3$ independent experiments). (**D**) Western blot analysis of the indicated proteins from the livers of ND- or HFD-fed mice ($n = 3$ mice per diet). (**E**) Absolute quantification of PKD isoform expression in the liver by quantitative polymerase chain reaction (QPCR) with in-exon primers and normalizing values to a genomic DNA standard ($n = 8$ biological replicates per group, combined data from three independent experiments). In (A) and (E), data are presented as means ± SEM. *$P > 0.05$ [unpaired two-tailed Student's *t* test (A) or one way ANOVA with post hoc Tukey's test (E)].

on the expression of lipogenic genes because stimulation of primary hepatocytes with the DAG analog decreased transcription of genes involved in de novo lipid synthesis (fig. S1C). Consistent with the results obtained from cultured hepatocytes, we observed increased PKD activity in the livers of HFD-fed mice compared with ND-fed animals (Fig. 1D and fig. S1D). Three PKD isoforms (PKD1, PKD2, and PKD3) have been identified so far (*8*). We did not detect *PKD1* mRNA in hepatocytes, and the expression of the *PKD2* isoform was marginal. However, we observed a robust expression of the *PKD3* isoform (Fig. 1E). Together, these data indicate that PKD3 could mediate the development of hepatic dysfunction in obese animals.

Hepatic deletion of PKD3 promotes insulin sensitivity

These results prompted us to generate mice deficient for PKD3 specifically in hepatocytes. We crossed PKD3 floxed mice (*PKD3*$^{f/f}$) (*20*) with a mouse strain expressing Cre recombinase under the control of the albumin promoter [B6.Cg-Tg(Alb-cre)21Mgn/J] (*21*). The resulting *PKD3*$^{liver\Delta/\Delta}$ mice showed specific deletion of PKD3 in the liver but not in other organs (fig. S2, A and B). *PKD3*$^{liver\Delta/\Delta}$ mice fed an ND or HFD gained similar amounts of body weight (BW) as control animals (Fig. 2A and fig. S3A). Mice deficient for PKD3 in hepatocytes presented with increased liver weight compared with control littermates when fed an HFD, whereas the weight of other organs was not affected (Fig. 2B). Similarly, all measured organ weights were not affected by PKD3 deletion in mice fed ND (fig. S3B). Consistently, energy expenditure, food intake, voluntary movements, and respiratory exchange ratio were not affected by hepatocyte-specific deletion of PKD3 in mice fed an HFD or ND (figs. S2, C to F, and S3, C to F). However, mice deficient for PKD3 in hepatocytes were partially protected from HFD-induced glucose intolerance and insulin resistance (Fig. 2, C and D, and fig. S2, G and H), whereas ND did not alter glucose or insulin sensitivity in these mice (fig. S3, G to J). Circulating insulin levels in mice deficient for hepatic PKD3 were significantly reduced (Fig. 2E), which is in line with the improved insulin sensitivity observed in these animals. Accordingly, the activation of the kinase AKT in response to insulin was enhanced in livers of HFD-fed *PKD3*$^{liver\Delta/\Delta}$ mice (Fig. 2, F and G). Together, these results indicate that deletion of PKD3 in hepatocytes partially restores insulin signaling attenuated by HFD feeding.

Deletion of PKD3 in hepatocytes promotes TG and cholesterol accumulation

The increased liver weight of *PKD3*$^{liver\Delta/\Delta}$ mice fed an HFD might be caused by enhanced proliferation of hepatocytes, decreased apoptosis, or increased lipid accumulation in the liver. Ki-67 staining, which marks proliferating cells, and cleaved caspase-3, which marks apoptotic cells, showed that PKD3 deficiency did not affect these processes in hepatocytes (fig. S4, A and B). Similarly, the number of apoptotic [terminal deoxynucleotidyl transferase–mediated deoxyuridine triphosphate nick end labeling (TUNEL)–positive] hepatocytes was similar between *PKD3*$^{liver\Delta/\Delta}$ mice and control animals (fig. S4, C and D). However, hematoxylin and eosin (H&E) staining of liver sections revealed an increased number and enlarged lipid droplets in *PKD3*$^{liver\Delta/\Delta}$ mice fed an HFD as compared with control animals (Fig. 3A), but no changes in the gross liver morphology of *PKD3*$^{liver\Delta/\Delta}$ mice fed an ND (fig. S3K). Accordingly, hepatic TG and total cholesterol content was markedly enhanced in *PKD3*$^{liver\Delta/\Delta}$ mice fed an HFD (Fig. 3, B and C), but not in those fed an ND (fig. S3, L and M). Thin-layer chromatography (TLC) analysis of neutral lipids isolated from the livers of *PKD3*$^{liver\Delta/\Delta}$ mice fed an HFD revealed markedly increased cholesteryl ester (CE) and TG content (Fig. 3, D to F). Circulating cholesterol levels were also increased in *PKD3*$^{liver\Delta/\Delta}$ mice fed an HFD (Fig. 3G), but not in those fed an ND (fig. S3, N and O). However, TG levels were not affected by an HFD in mice deficient for PKD3 (Fig. 3H).

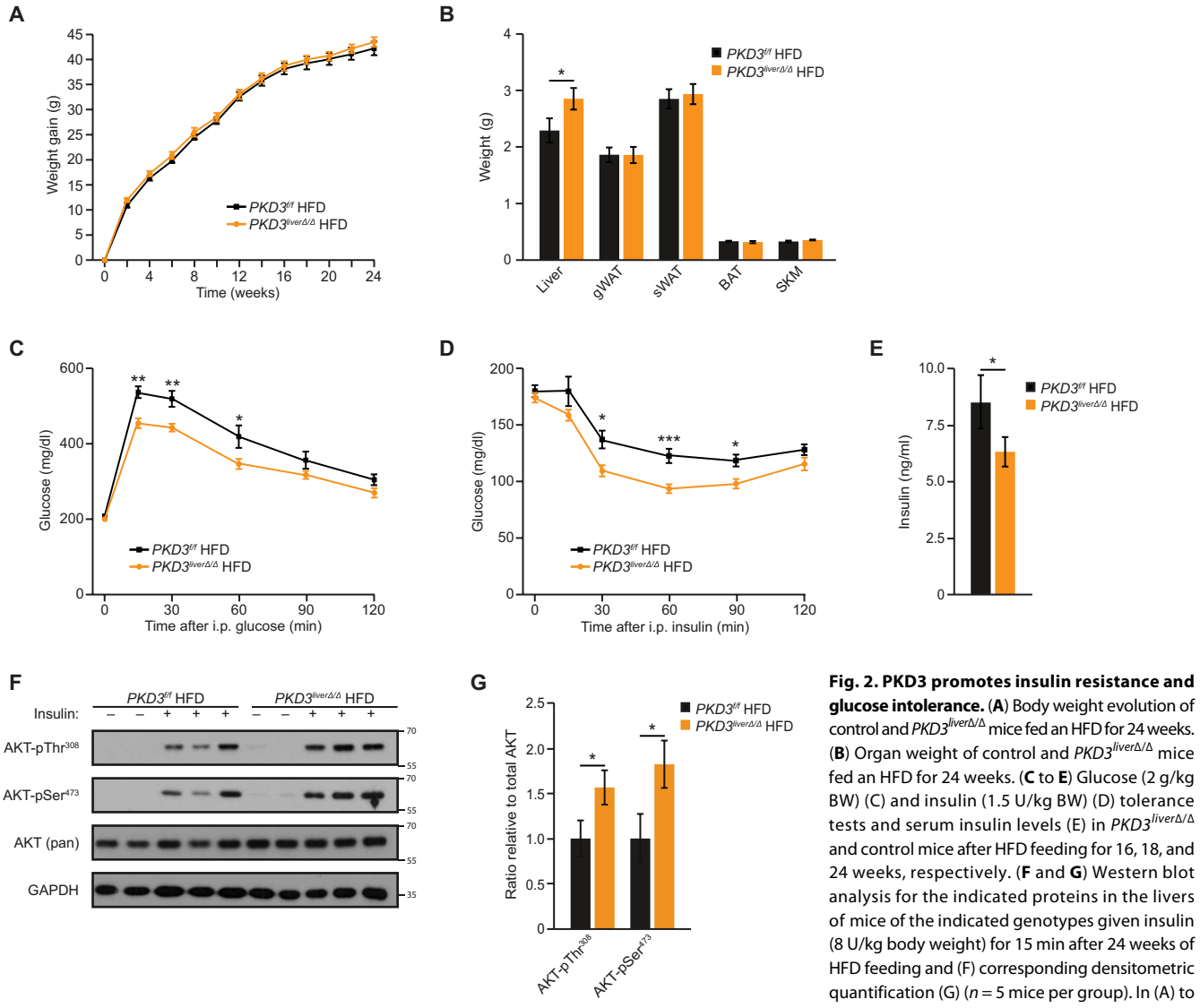

Fig. 2. PKD3 promotes insulin resistance and glucose intolerance. (**A**) Body weight evolution of control and $PKD3^{liver\Delta/\Delta}$ mice fed an HFD for 24 weeks. (**B**) Organ weight of control and $PKD3^{liver\Delta/\Delta}$ mice fed an HFD for 24 weeks. (**C** to **E**) Glucose (2 g/kg BW) (C) and insulin (1.5 U/kg BW) (D) tolerance tests and serum insulin levels (E) in $PKD3^{liver\Delta/\Delta}$ and control mice after HFD feeding for 16, 18, and 24 weeks, respectively. (**F** and **G**) Western blot analysis for the indicated proteins in the livers of mice of the indicated genotypes given insulin (8 U/kg body weight) for 15 min after 24 weeks of HFD feeding and (F) corresponding densitometric quantification (G) ($n = 5$ mice per group). In (A) to (E), $n = 8$ mice [wild type (WT)] and $n = 15$ mice [knockout (KO)] were used, and in (A) to (E) and (G), data are presented as means ± SEM. $^*P > 0.05$, $^{**}P > 0.01$, and $^{***}P > 0.001$ [unpaired two-tailed Student's t test (B and E), one-way ANOVA with post hoc Tukey's test (G), or two-way ANOVA with post hoc Tukey's test (A, C, and D)]. i.p., intraperitoneal; GAPDH, glyceraldehyde-3-phosphate dehydrogenase.

Increased lipid accumulation characterizes steatosis and NAFLD, which progresses into NASH upon the infiltration of immune cells, and into cirrhosis upon the induction of fibrosis (*22*). As assessed by immunohistochemistry, infiltration of macrophages (F4/80), T cells (CD3), or B cells (B220) was not altered in the livers from $PKD3^{liver\Delta/\Delta}$ animals fed an HFD compared with control mice (fig. S4A). Similarly, collagen type IV and Sirius red staining revealed that the extent of fibrosis was similar between HFD-fed $PKD3^{liver\Delta/\Delta}$ and control animals. Together, these results indicate that hepatic PKD3 suppresses cholesterol and TG accumulation in the liver and, therefore, protects against the development of fatty liver disease.

PKD3 suppresses de novo lipid synthesis in hepatocytes

To unravel the cause for increased lipid accumulation in PKD3-deficient livers, we isolated primary hepatocytes and measured the rates of de novo lipogenesis and fatty acid (FA) oxidation. In parallel, we also assessed very low density lipoprotein (VLDL) secretion in $PKD3^{liver\Delta/\Delta}$ mice fed an HFD and ND. Overall, de novo lipid synthesis was increased in hepatocytes deficient for PKD3 under basal and insulin-stimulated conditions (Fig. 4A), whereas FA oxidation was moderately increased despite higher lipid accumulation in $PKD3^{liver\Delta/\Delta}$ mice (fig. S5A). To determine VLDL secretion, we performed tyloxapol injection (to inhibit lipoprotein lipase, which results in blocked peripheral lipid uptake). We did not observe alterations in TG levels between $PKD3^{liver\Delta/\Delta}$ and control animals regardless of the diet (fig. S5, B and C). To further investigate increased de novo lipogenesis, we performed TLC-based separation of the major lipid classes. In the absence of PDK3, we observed increased synthesis rates of cholesterol [both free cholesterol (FC) and CEs] and TGs, whereas the synthesis of other lipids [free fatty acids (FFAs), phosphatidylethanolamine (PE),

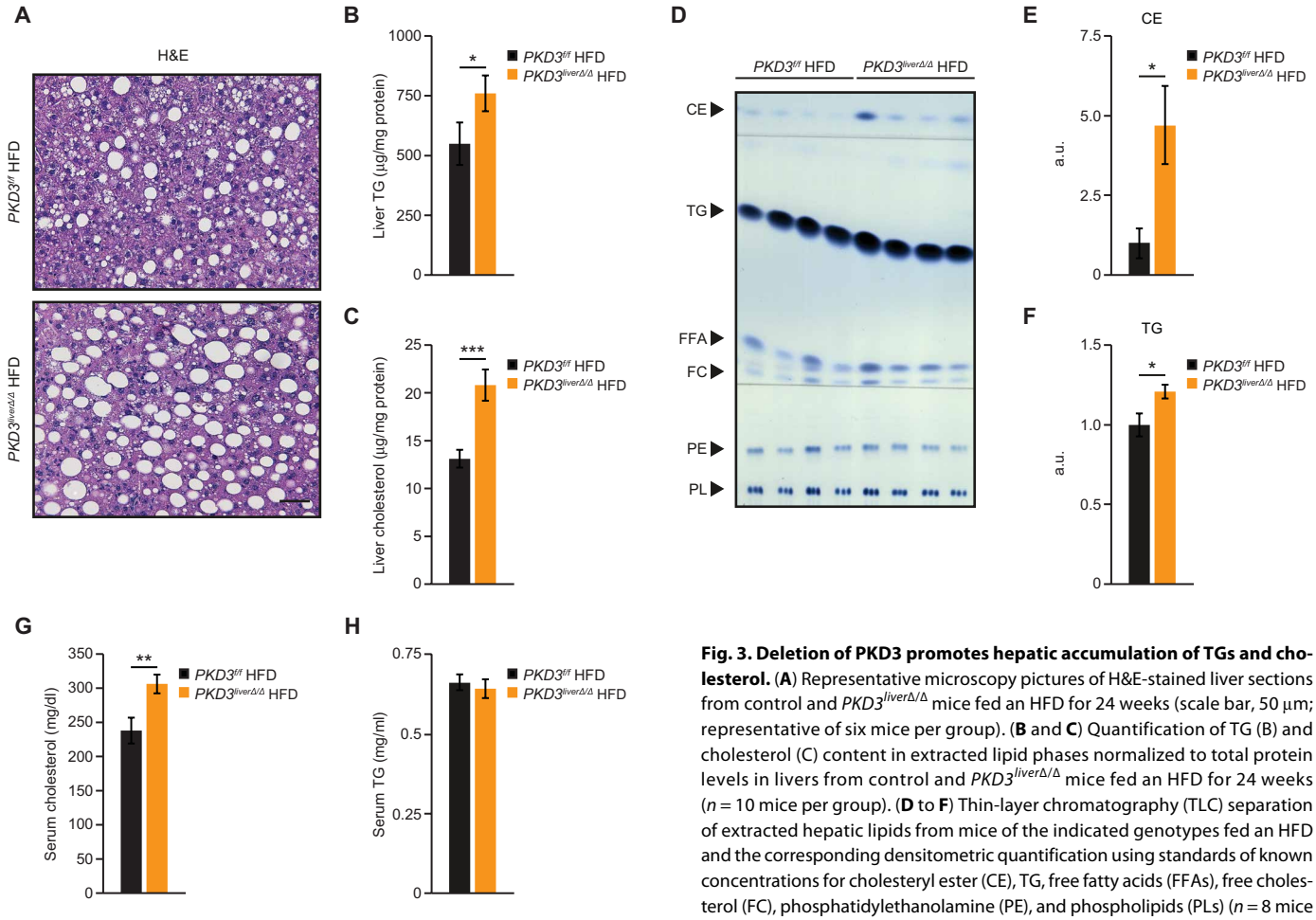

Fig. 3. Deletion of PKD3 promotes hepatic accumulation of TGs and cholesterol. (**A**) Representative microscopy pictures of H&E-stained liver sections from control and *PKD3*$^{liver\Delta/\Delta}$ mice fed an HFD for 24 weeks (scale bar, 50 μm; representative of six mice per group). (**B** and **C**) Quantification of TG (B) and cholesterol (C) content in extracted lipid phases normalized to total protein levels in livers from control and *PKD3*$^{liver\Delta/\Delta}$ mice fed an HFD for 24 weeks ($n = 10$ mice per group). (**D** to **F**) Thin-layer chromatography (TLC) separation of extracted hepatic lipids from mice of the indicated genotypes fed an HFD and the corresponding densitometric quantification using standards of known concentrations for cholesteryl ester (CE), TG, free fatty acids (FFAs), free cholesterol (FC), phosphatidylethanolamine (PE), and phospholipids (PLs) ($n = 8$ mice per group). (**G** and **H**) Quantification of serum cholesterol (G) and serum TG (H) concentrations in control and *PKD3*$^{liver\Delta/\Delta}$ mice fed an HFD for 20 weeks ($n = 8$ mice per group). In (B), (C), and (E) to (H), data are presented as means ± SEM. *$P > 0.05$, **$P > 0.01$, and ***$P > 0.001$ (unpaired two-tailed Student's *t* test). a.u., arbitrary unit.

and phospholipids (PLs)] was not affected (Fig. 4B). Increased de novo lipogenesis was also observed in vivo in *PKD3*$^{liver\Delta/\Delta}$ mice, which synthesized significantly more lipids in the liver under lipogenic conditions compared with control mice when fed an HFD (Fig. 4C). SREBPs are master regulators of transcription of genes involved in hepatic FAs and cholesterol synthesis (*3*). The level of the cleaved and mature form of SREBP1, which promotes lipogenic gene expression and its own mRNA levels (*3*), was increased in PKD3-deficient hepatocytes compared with wild-type hepatocytes (Fig. 4D and fig. S5D). Consistently, transcriptional analysis revealed increased levels of *Srebp1c* and *Srebp2* and their target genes—*Acaca* (which encodes acetyl-CoA carboxylase alpha), *Fasn* (which encodes FA synthase), *Scd1* (which encodes stearoyl-CoA desaturase), *Hmgcs1* (which encodes 3-hydroxyl-3-methylglutaryl-CoA synthase 1), *Hmgcr* (which encodes 3-hydroxyl-3-methylglutaryl-CoA reductase), *Mvk* (which encodes mevalonate kinase), *Mvd* (which encodes mevalonate diphosphate decarboxylase), *Fdps* (which encodes farnesyl diphosphate synthase), *Fdft1* (which encodes farnesyl-diphosphate farnesyltransferase 1), *Lss* (which encodes lanosterol synthase), and *Dhcr7* (which encodes 7-dehydrocholesterol reductase)—in hepatocytes deficient for PKD3 (Fig. 4E). Correspondingly, mRNA and protein levels of factors promoting lipogenesis were also increased in the livers of *PKD3*$^{liver\Delta/\Delta}$ mice compared with control animals when fed an HFD (Fig. 4, F and G, and fig. S5E). Conversely, *Srebp1c* and *Srebp2* silencing abolished the significant difference in gene expression of lipogenic genes in PKD3-deficient compared with wild-type hepatocytes (Fig. 4H and fig. S5F). Moreover, the PKD-specific inhibitor CRT0066101 increased the mRNA expression of *Srebp1c*, *Srebp2*, *Hmgcr*, and *Fdps* under insulin-stimulated conditions in primary hepatocytes and brought them to the same level as in PKD3-deficient hepatocytes without or with inhibitor (Fig. 5A). Accordingly, administration of the PKD inhibitor significantly increased the hepatic expression of *Srebp1c*, *Srebp2*, and their target genes (Fig. 5B).

Under physiological conditions, hepatic lipogenesis and the expression of genes promoting this process are induced upon feeding. The expression of *Srebp1c*, *Srebp2*, and some of their transcriptional targets were also increased in the livers of PKD3-deficient mice subjected to a fasting/refeeding protocol (Fig. 5C), whereas under fasting conditions, expression of lipogenic genes was not affected by PKD3 deletion (fig. S5G). Moreover, the expression of *Insig1* (insulin-induced gene 1) and *Insig2*, which encode proteins that prevent the proteolytic cleavage of SREPP, did not differ between *PKD3*$^{liver\Delta/\Delta}$ and control mice (Fig. 5C and fig. S5G). PKD3 protein level in the liver was increased upon prolonged refeeding after fasting, but PKD3 abundance

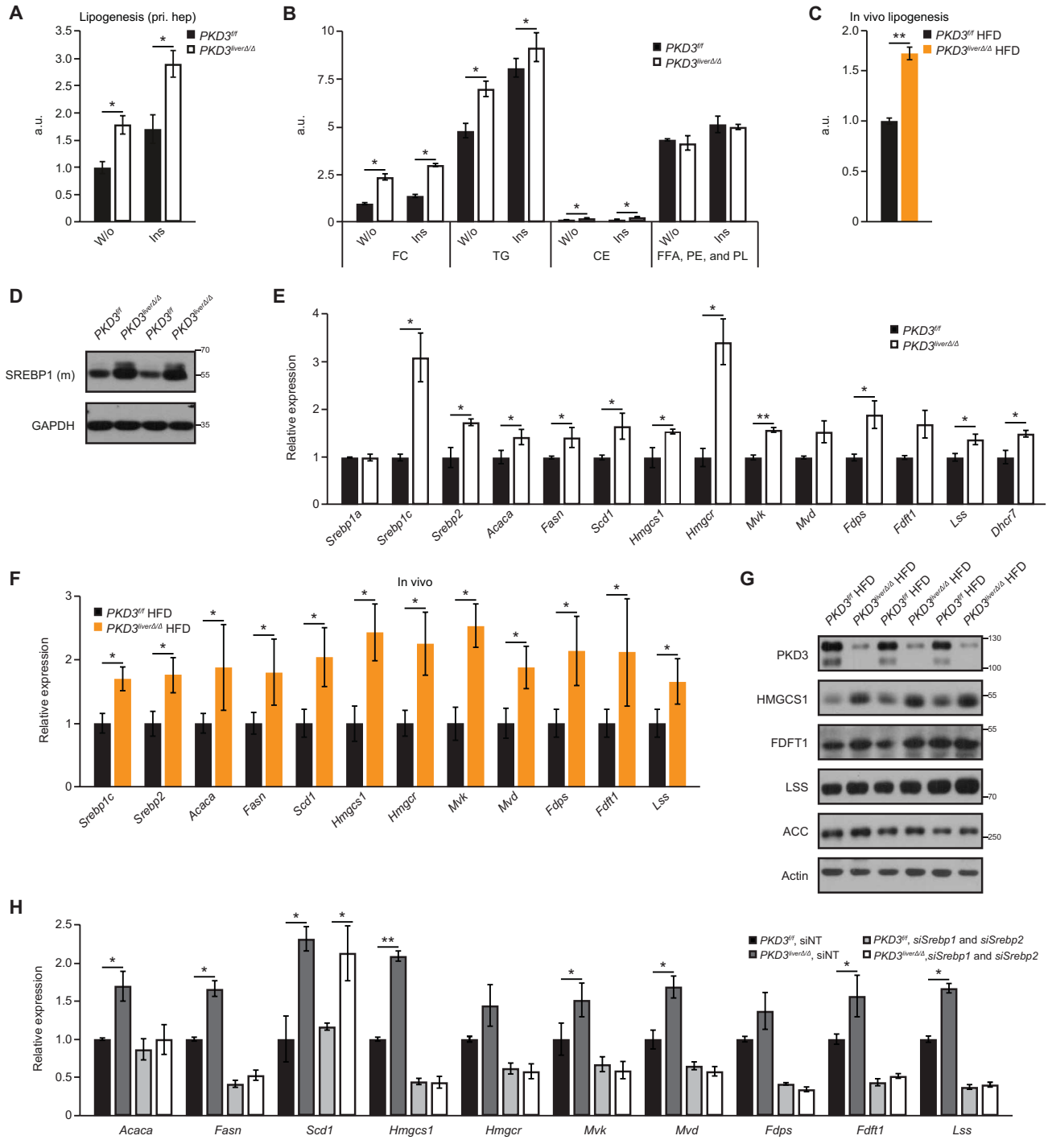

Fig. 4. Hepatic PKD3 suppresses de novo lipogenesis in a SREBP-dependent manner. (**A** and **B**) Basal and insulin-induced total de novo lipogenesis rate (measured under lipogenic conditions: serum deprived, 25 mM glucose, 0.5 mM sodium acetate, and 100 nM insulin) in primary hepatocytes isolated from mice of the indicated genotypes (a.u.) (A) and quantification of TLC-separated FC, TG, CE, and other lipids (FFA, PE, and PL) (B) ($n = 3$ biological replicates per group). (**C**) In vivo de novo lipogenesis rate (a.u.) in livers from control and *PKD3*$^{liver\Delta/\Delta}$ mice fed an HFD for 8 weeks, fasted overnight, and refed for 4 hours before analysis ($n = 5$ mice per group). (**D**) Western blot analysis of mature SREBP1 in primary hepatocytes of the indicated genotypes under the same lipogenic conditions as in (B) ($n = 3$ mice per group; representative of three individual experiments). (**E**) QPCR analysis of *Srebp* gene and target gene expression in primary hepatocytes of the indicated genotypes under the same lipogenic conditions as in (B) ($n = 3$ mice per group). (**F**) QPCR analysis of *Srebp* gene and target gene expression in livers from control and *PKD3*$^{liver\Delta/\Delta}$ mice fed for 20 weeks with HFD, subjected to fasting overnight and refeeding for 4 hours ($n = 6$ mice per group). (**G**) Western blot analysis for indicated proteins in livers from the mice in (F) ($n = 3$ mice per group). (**H**) QPCR analysis of *Srebp* gene and target gene expression in primary hepatocytes of the indicated genotypes stimulated with insulin for 4 hours that were either transfected with siNonTargeting (siNT) or the combination of *siSrebp1* and *siSrebp2* as indicated ($n = 3$ biological replicates per condition). In (A) to (C), (E), (F), and (H), data are presented as means ± SEM. *$P > 0.05$ and **$P > 0.01$ [unpaired two-tailed Student's *t* test (C, E, and F) or one-way ANOVA with post hoc Tukey's test (A, B, and H)].

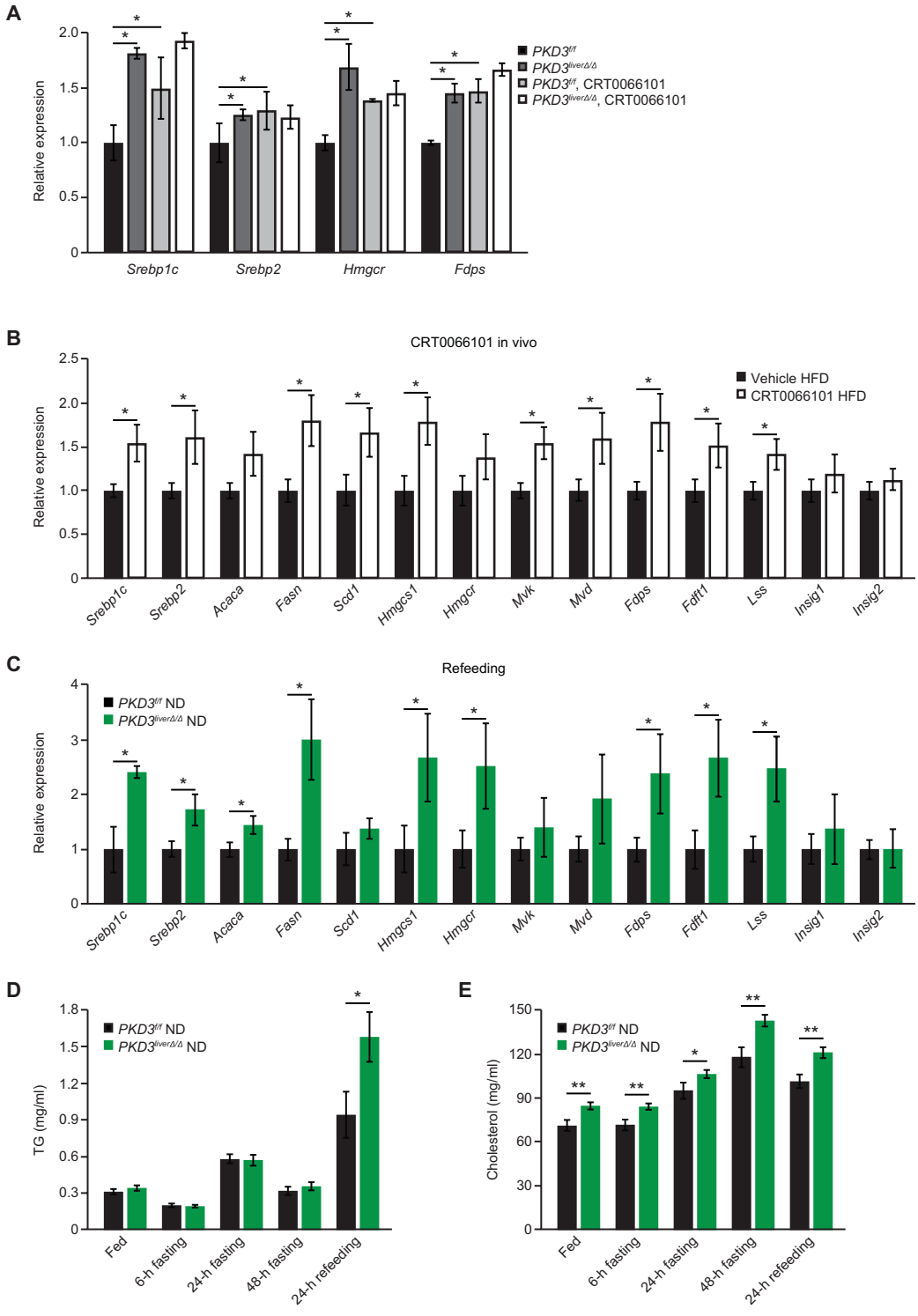

Fig. 5. The effect of the PKD inhibitor CRT0066101 and refeeding on lipogenic gene expression and hepatic lipid accumulation. (**A**) QPCR analysis of insulin-stimulated *Srebp1c* expression in DMSO or CRT0066101 (0.1 μM)–treated primary hepatocytes of the indicated genotypes ($n = 3$ biological replicates per condition). (**B**) QPCR analysis of the expression of *Srebp* and target genes in the livers from HFD-fed C57BL/6JRj mice (for 8 weeks) that either received an intraperitoneal injection of vehicle or CRT0066101 (10 mg/kg BW) inhibitor for five consecutive days. Mice were fasted overnight and refed for 4 hours before the livers were excised ($n = 8$ mice per group). (**C**) QPCR analysis of the indicated genes in the livers from control and *PKD3*$^{liverΔ/Δ}$ mice after overnight fasting and refeeding for 4 hours ($n = 4$ mice per group; combined data from two individual experiments). (**D** and **E**) Quantification of serum TG (D) and serum cholesterol (E) concentrations at the indicated time points in control and *PKD3*$^{liverΔ/Δ}$ mice fed an ND for 7 weeks that were fasted and refed for the indicated time points ($n = 12$ mice per group). In (A) to (E), data are presented as means ± SEM. *$P > 0.05$ and **$P > 0.01$ [unpaired two-tailed Student's *t* test (B and C), one-way ANOVA with post hoc Tukey's test (A), or two-way ANOVA with post hoc Tukey's test (D and E)].

and phosphorylation were not affected shortly (within 4 hours) after food consumption (fig. S5, H to K). Last, serum TG and cholesterol levels were increased by fasting, followed by 24 hours of refeeding in *PKD3*$^{liver\Delta/\Delta}$ mice (Fig. 5, D and E), indicating that PKD3 limits lipid synthesis evoked by feeding. Together, these data indicate that PKD3 suppresses de novo cholesterol and TG production by attenuating SREBP-dependent transcription of enzymes required for these processes.

PKD3 attenuates the expression of lipogenic genes in an AKT- and mTORC1/2-dependent manner

Insulin-stimulated activation of SREBP1c-dependent transcription relies on AKT activation (*3*, *23*–*25*). We observed increased insulin-stimulated phosphorylation of AKT at Ser^{473} and Thr^{308} in hepatocytes deficient for PKD3 compared with control cells (Fig. 6A and fig. S7A). To check if PKD3 activation is sufficient to suppress insulin signaling, we created hepatocytes expressing a constitutively active form of PKD3 (mycPKD3ca), in which the two serine residues in the kinase domain are mutated to glutamic acid (S731E/S735E) (figs. S6C and S8A) (*26*). This mutation leads to the activation of PKD3 regardless of the upstream signaling events. Consistent with previous results, expression of mycPKD3ca in hepatocytes reduced the phosphorylation of AKT at Ser^{473} and Thr^{308} upon insulin stimulation (Fig. 6B and fig. S8B).

Insulin-evoked induction of lipogenesis requires the activation of downstream effectors of AKT. This includes activation of mTORC1 and mTORC2, which are required for SREBP1c activation and promote its transcription (*4*, *27*–*29*). We observed enhanced phosphorylation of mTORC1 target ribosomal protein S6 kinase beta-1 (S6K1) on Thr^{389} and phosphorylation of 4E-BP1 on Thr$^{37/46}$ and Ser^{65} in hepatocytes deficient for PKD3 (Fig. 6C and fig. S7B). Similarly, phosphorylation of downstream targets of mTORC2 such as serum/glucocorticoid-regulated kinase 1 (SGK1) on Ser^{422} and N-Myc downstream regulated target 1 (NDRG1) on Thr^{346} was also increased in the absence of PKD3 (Fig. 6C and fig. S7B). Phosphorylation of AKT on Ser^{473}, which is a direct target of mTORC2, was also increased in hepatocytes in the absence of PKD3 (Fig. 6A and fig. S7A). The abundance and/or phosphorylation of other components of mTORC1 and mTORC2 was not affected by deletion of PKD3 (figs. S6A and S7C). Next, we loaded primary hepatocytes with oleic acid to mimic an HFD in vitro. Under this condition, deletion of PKD3 resulted in increased phosphorylation of AKT on Ser^{473} and Thr^{308}, 4E-BP1 on Thr$^{37/46}$ and Ser^{65}, SGK1 on Ser^{422}, and NDRG1 on Thr^{346} (figs. S6B and S7, D and E). Conversely, expression of mycPKD3ca in hepatocytes resulted in decreased phosphorylation of mTORC1 targets (S6K1 on Thr^{389} and 4E-BP1 on Thr$^{37/46}$ and Ser^{65}) and mTORC2 targets (NDRG1 on Thr^{346} and AKT on Ser^{473}) (Fig. 6, B and D, and fig. S8, B and C). However, the abundance of other mTORC1 and mTORC2 components was not affected by the expression of mycPKD3ca (figs. S6D and S8, D and E), although the total protein level of NDRG1 was increased in hepatocytes expressing mycPKD3ca (Fig. 6D). Accordingly, the phosphorylation of S6K1 on Thr^{389}, NDRG1 on Thr^{346}, and SGK1 on Ser^{422} were also increased in the livers of HFD-fed *PKD3*$^{liver\Delta/\Delta}$ mice that received insulin (figs. S6E and S8F). Phosphorylation of the insulin receptor substrate at Ser^{612} was increased in hepatocytes expressing mycPKD3ca (fig. S6D), which indicates that other signaling pathways might be activated by the expression of PKD3. Together, these data indicate that PKD3 suppresses lipogenesis by attenuating AKT-, mTORC1-, and mTORC2-dependent signaling.

To support this notion, we measured the lipogenesis rate in hepatocytes treated with the PKD inhibitor CRT0066101 in combination with compounds that block the activity of AKT (Akti-1/2), mTORC1 (rapamycin), and mTORC1/2 (KU0063794) (Fig. 6E). As expected, inhibition of PKD increased the lipogenesis rate, and the addition of the AKT inhibitor resulted in similar inhibition of lipid synthesis in control and CRT0066101-treated hepatocytes (Fig. 6E). Similarly, an mTORC1/2 inhibitor (KU0063794) decreased lipogenesis in control and CRT0066101-treated cells to the same extent (Fig. 6E). However, rapamycin treatment only partially inhibited lipogenesis in CRT0066101-treated cells compared with control cells (Fig. 6E).

The closely related PKD1 isoform promotes lipogenesis in adipocytes by phosphorylating 5′-adenosine monophosphate (AMP)–activated protein kinase (AMPK) and suppressing its activity toward acetyl-CoA carboxylase 1/2 (ACC1/2) (*19*). However, our data suggest that PKD3 does not affect AMPK or ACC1/2 activity in hepatocytes (figs. S6D and S8E) but attenuates AKT- and mTORC1/2-driven lipogenesis.

Constitutive activation of PKD3 promotes insulin resistance in the liver

To analyze the effect of moderate overexpression of PKD3ca on insulin signaling in vivo, we generated loxP-STOP-loxP-FlagPKD3ca mice and crossed them with mice expressing Cre recombinase under the control of the albumin promoter (*21*) to restrict the expression of PKD3ca to hepatocytes. Liver-specific transgenic PKD3ca mice (*TgPKD3ca*^{liver}) showed impaired glucose tolerance (Fig. 7A and fig. S9A), which was accompanied by reduced insulin sensitivity even when these mice were fed an ND (Fig. 7B and fig. S9B). Accordingly, these observations were also reflected by increased fasting glucose and fasting insulin levels (Fig. 7, C and D). Overall, *TgPKD3ca*^{liver} mice presented with pronounced insulin resistance as shown by a homeostatic model assessment for insulin resistance (HOMA-IR) index of 2.5 (Fig. 7E). Consistent with the results obtained from the isolated hepatocytes, we observed reduced phosphorylation of AKT on Ser^{473} and Thr^{308} in the livers from *TgPKD3ca*^{liver} mice that were refed (Fig. 7, F and G). Expression of lipogenic genes was only marginally reduced, whereas liver TG and cholesterol content were not significantly reduced ($P = 0.64$ and $P = 0.08$, respectively) in *TgPKD3ca*^{liver} mice when fed an ND (fig. S9, C to E). Together, these data suggest that activation of PKD3 alone is sufficient to suppress insulin signaling (Fig. 7H).

DISCUSSION

DAG-evoked activation of PKC-dependent signaling is critical for the development of hepatic insulin resistance (*2*, *5*–*7*). Our study revealed PKD3 as a mediator of DAG-evoked insulin resistance in the liver. DAG is an intermediate product of TG synthesis, but it is also used by a subclass of G protein (heterotrimeric GTP-binding protein)–coupled receptors as a second messenger (*5*). Our data also demonstrated that PKD3 was activated in the livers of obese (HFD fed) mice. Moreover, lipid loading of primary hepatocytes and stimulation of cells with insulin resulted in activation of PKD3. However, the precise upstream mechanism promoting PKD3 activation and the relationship of this kinase to the classical PKC-dependent signaling pathway require further investigation.

Although we showed that PKD3 is one of the signaling molecules aberrantly activated during metabolic overload evoked by high levels of lipids supplementation and its deletion partially ameliorated

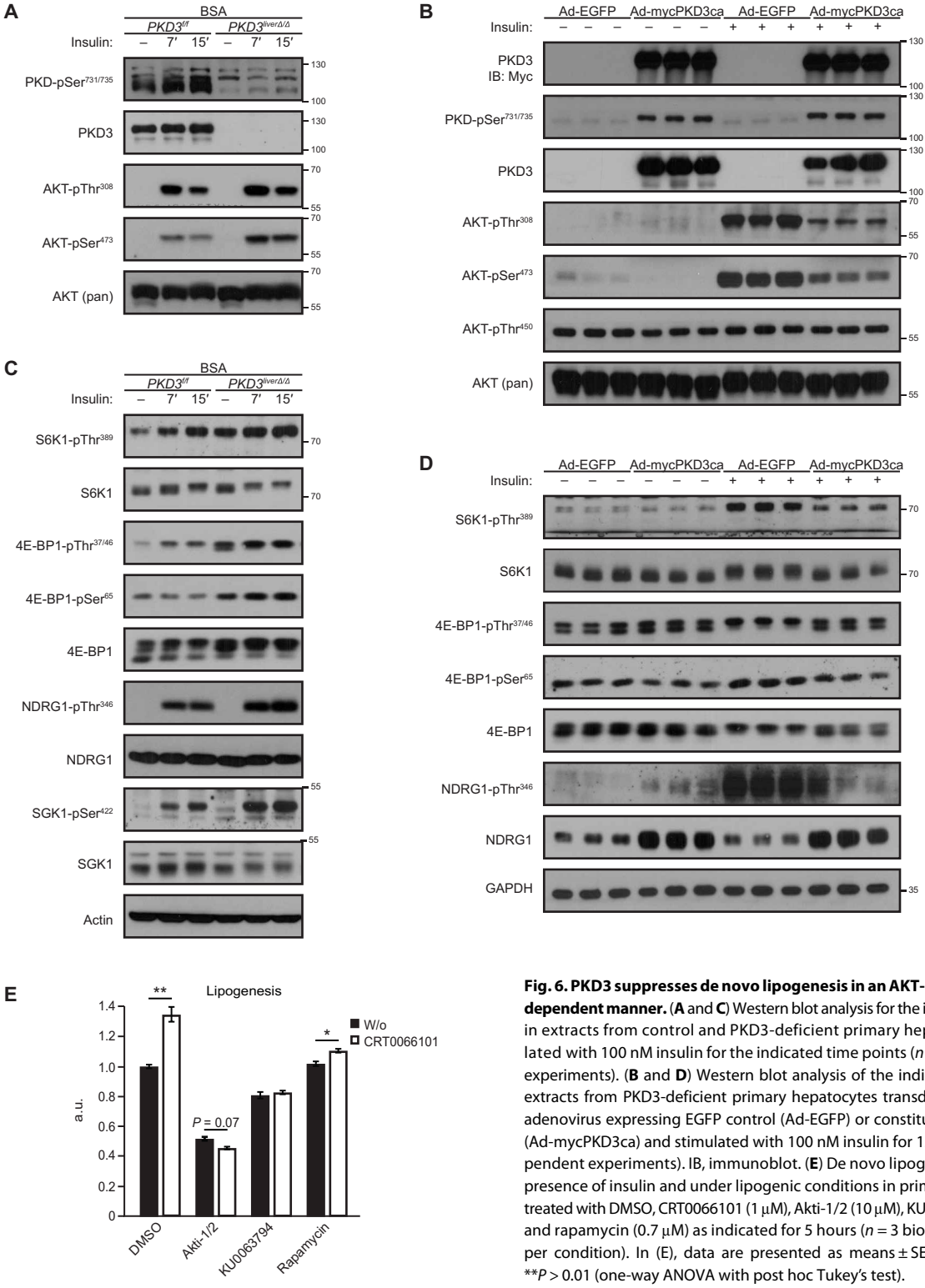

Fig. 6. PKD3 suppresses de novo lipogenesis in an AKT- and mTORC1/2-dependent manner. (**A** and **C**) Western blot analysis for the indicated proteins in extracts from control and PKD3-deficient primary hepatocytes stimulated with 100 nM insulin for the indicated time points ($n = 3$ independent experiments). (**B** and **D**) Western blot analysis of the indicated proteins in extracts from PKD3-deficient primary hepatocytes transduced with either adenovirus expressing EGFP control (Ad-EGFP) or constitutive active PKD3 (Ad-mycPKD3ca) and stimulated with 100 nM insulin for 15 min ($n = 3$ independent experiments). IB, immunoblot. (**E**) De novo lipogenesis rate in the presence of insulin and under lipogenic conditions in primary hepatocytes treated with DMSO, CRT0066101 (1 μM), Akti-1/2 (10 μM), KU0063794 (0.7 μM), and rapamycin (0.7 μM) as indicated for 5 hours ($n = 3$ biological replicates per condition). In (E), data are presented as means ± SEM. *$P > 0.05$ and **$P > 0.01$ (one-way ANOVA with post hoc Tukey's test).

insulin resistance caused by lipid overload, PKD3 seems to also have a physiological function in the liver. We revealed that PKD3 expression was important to provide a negative feedback loop on lipogenesis evoked by refeeding after fasting/starvation, which would be in line with the increase in PKD3 abundance in response to prolonged refeeding and the increase in PKD activity in response to insulin stimulation.

PKCε suppresses insulin action by directly phosphorylating the insulin receptor (*6*, *7*). Our data suggest that PKD3 also suppressed insulin action, resulting in impaired AKT phosphorylation and

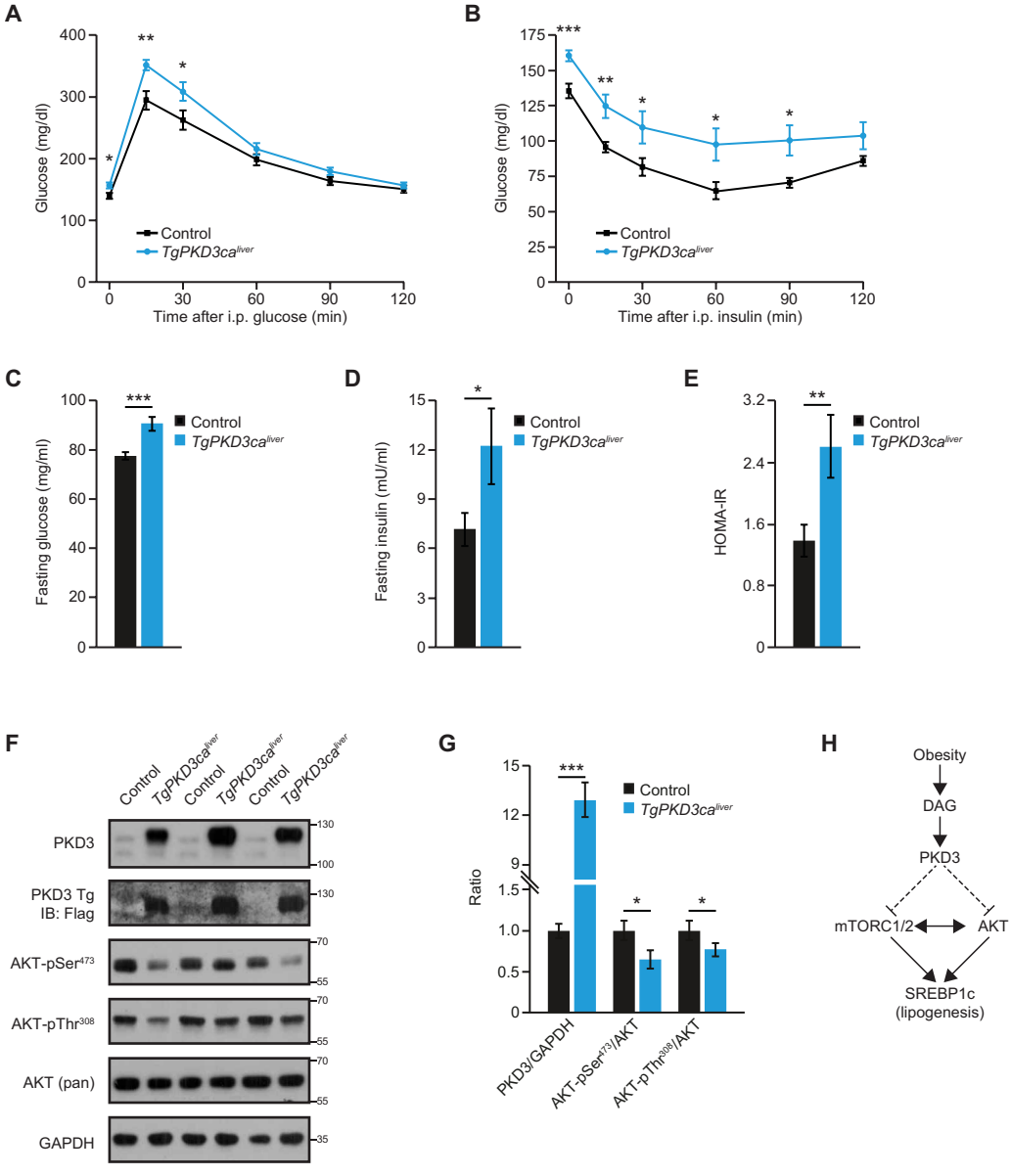

Fig. 7. Liver-specific expression of constitutively active PKD3 promotes insulin resistance. (**A** and **B**) Glucose (2 g/kg BW) (A) and insulin (1 U/kg BW) (B) tolerance test in *TgPKD3ca*^{liver} and control mice fed an ND for 12 and 10 weeks, respectively [$n = 11$ mice (control) and $n = 13$ mice (Tg)]. (**C** to **E**) After overnight fast, blood glucose (C) and serum insulin (D) were measured and used to determine HOMA-IR (E) in mice of the indicated genotypes [$n = 11$ mice (control) and $n = 13$ mice (Tg)]. (**F** and **G**) Western blot analysis of the indicated proteins from livers of mice of the indicated genotypes that were fasted overnight and refed 4 hours before analysis (F) and corresponding densitometric quantification (G) ($n = 3$ mice per group). (**H**) Summary of PKD3 signaling in the liver. In (A) to (E) and (G), data are presented as means ± SEM. $^*P > 0.05$, $^{**}P > 0.01$, and $^{***}P > 0.001$ [unpaired two-tailed Student's *t* test (C to E and G) or two-way ANOVA with post hoc Tukey's test (A and B)].

reduced mTORC1 and mTORC2 activation in vitro and in vivo. Hepatic deletion of PKD3 not only improved glucose tolerance in mice but also resulted in an increased SREBP-dependent lipogenesis and, consequently, hepatic accumulation of TG and cholesterol. SREBP1c and SREBP2 are critical for the transcriptional activation of lipogenic machinery in hepatocytes (*3*). However, the phosphorylation of the mTORC2 downstream effector NDRG1 promotes lipogenesis in a PPARγ (peroxisome proliferator–activated receptor γ)–dependent manner in adipocytes (*30*). We found that phosphorylation of NDRG1 was enhanced in the absence of PKD3, suggesting that PKD3 might suppress lipogenesis by using mechanisms complementary to the suppression of SREBP-dependent transcription of lipogenic genes. Similarly, PKD3-dependent suppression of AKT and mTORC1/2 actions might influence lipogenesis by inhibiting factors such as DNA-dependent protein kinase (DNA-PK) or upstream stimulatory factors (USF), which also promote the expression of lipogenic enzymes (*31*). However, we showed that silencing of SREBP isoforms was sufficient to normalize the elevated rates of lipogenesis in PKD3-deficient hepatocytes, which indicates that PKD3 regulates lipogenesis primarily by suppressing SREBP-dependent transcription of lipogenic genes. PKD3 did not affect TG secretion in the form of VLDLs from hepatocytes. Moreover, deletion of PKD3 seemed to increase FA oxidation

in hepatocytes. Increased rates of FA oxidation in hepatocytes would be expected to lead to reduced TG content in the liver. However, lipid accumulation in the livers of PKD3-deficient mice, despite increased FA oxidation and unaffected rates of VLDL secretion, indicates that elevated lipogenesis is the primary process responsible for the observed phenotype. Although the closely related PKD1 promotes lipid accumulation in adipocytes in an AMPK-dependent manner (*19*), PKD3 did not affect the activity of AMPK or its downstream target ACC1/2 in the liver. In addition, PKD3 seemed to be the predominant PKD isoform that regulates liver metabolism because PKD inhibition did not further stimulate expression of lipogenic genes in the absence of PKD3 and other PKD isoforms were only marginally expressed in hepatocytes. Therefore, our results suggest that different PKD isoforms have a specific set of substrates in different tissues.

Our results also indicate that the expression of the constitutively active form of PKD3 was sufficient to attenuate insulin signaling (AKT and TORC1/2 activity) even in the absence of hyperlipidemia. Mice expressing the constitutively active form of PKD3 in the liver showed reduced insulin sensitivity and reduced AKT phosphorylation even when fed an ND. Cholesterol and TG content was not altered in these livers, and the expression of some SREBP target genes was only marginally reduced (fig. S9, C to E). These results might imply that increased insulin signaling is sufficient to enhance lipogenesis but that reducing insulin signaling does not necessarily block the lipogenic program. Alternatively, the ability of PKD3 to attenuate insulin signaling on lipogenesis might be present only in the livers of animals challenged with HFD.

Multiple studies report that hepatic TG and cholesterol levels correlate with the development of insulin resistance [reviewed in (*2*)]. However, we found that deletion of PKD3 promoted glucose use and insulin sensitivity while, at the same time, enhancing lipid accumulation in the liver. Improved glucose use and increased lipid deposition are observed in several mouse models in which AKT activity is increased (*23*, *32*). Nevertheless, we did not observe increases in apoptosis, immune cell infiltration, or fibrosis in PKD3-deficient livers, which are often associated with the progression of NAFLD into NASH (*2*). Therefore, PKD3 deletion results in the development of a metabolically healthy fatty liver.

Last, our data indicate that the expression of the constitutively active form of PKD3, which preserves its activity in hepatocytes of animals independently of hormonal or metabolic challenges, suppressed insulin signaling and induced insulin resistance and glucose intolerance. The expression of PKD3ca in hepatocytes not only suppressed AKT- and mTORC-dependent signaling but also led to phosphorylation of the insulin receptor substrate at Ser^{612}, which indicates that other signaling pathways [for example, mitogen-activated protein kinases (*33*)] might be activated by the expression of PKD3. Together, these data indicate that not only is PKD3 expression required to provide negative feedback on insulin signaling under conditions of lipid overload, but also its activation is sufficient to partially switch off insulin-dependent signaling.

MATERIAL AND METHODS

DAG quantification

DAG analysis was performed as described in detail before (*19*). Briefly, lipids were isolated from liver homogenates by the butanol-methanol extraction method. 1,2-Dioctanoyl-*sn*-glycerol (Enzo Life Sciences) was used as internal standard. Subsequently, lipid extracts were fractionated into lipid classes on a silica matrix column (Phenomenex), and the DAG fraction was analyzed by liquid chromatography–mass spectrometry (LC-MS).

Animals

PKD3 floxed mice ($PKD3^{f/f}$) (*20*) and loxP-STOP-loxP-(3xFlag)PKD3ca mice, in which the two serines in the PKD3 kinase domain are mutated to glutamic acid (S731E/S735E) (generated by Cyagen with the PiggyBac transgenic method), were mated with mice expressing transgenic Cre recombinase under the control of the albumin promoter/enhancer (the Jackson laboratory) (*21*) to generate homozygous liver-specific PKD3-deficient mice ($PKD3^{liver\Delta/\Delta}$) and heterozygous liver-specific transgenic PKD3ca mice ($TgPKD3ca^{liver}$), respectively. All animal studies were approved by the local animal welfare authorities (Regierung von Unterfranken) with the animal protocol nos. AK55.2-2531.01-124/13 and AK55.2.2-2532-2-741-13. The mice were housed in cages from Tecniplast in a green line IVC rack system with ad libitum supply of water and normal chow diet (ssniff Spezialdiaeten). In that case of HFD (Research Diets, D12331i), mice received the high-calorie diet (58% kcal from fat) from the age of 3 weeks for a duration of 24 weeks, and BW measurements were performed weekly. For dissection, mice were sacrificed by cervical dislocation, and organs [liver, gonadal white adipose tissue (gWAT), subcutaneous white adipose tissue (sWAT), brown adipose tissue (BAT), and skeletal muscle (SKM)] were weighted and snap frozen in liquid nitrogen. For fasting/refeeding experiments, mice were fasted overnight for 16 hours with free access to water, and food was restored for 4 hours before livers were removed as described before. For insulin injections, mice received an intraperitoneal dose of 8 U/kg BW of insulin (Sigma), and livers were collected after 15 min according to standard procedures. For in vivo experiments using CRT0066101, C57BL/6JRj mice (Janvier Labs) were fed an HFD for 8 weeks and were randomly assigned to two groups that either received an intraperitoneal injection 10 mg/kg BW of CRT0066101 in 5% dimethyl sulfoxide (DMSO) or vehicle for five consecutive days.

Glucose and insulin tolerance tests

For glucose tolerance tests, mice were fasted for 4 hours before the experiment (starting at 8:00 a.m.) and received an intraperitoneal injection of a defined dose of glucose (Carl Roth) as indicated in the figure legends. Glucose concentrations in the blood were measured with Accu-Chek glucometer (Roche) at 0-, 15-, 30-, 60-, 90-, and 120-min time points. Insulin tolerance tests were performed similarly, except that the mice received a defined dose of insulin (Sigma) as indicated in the figure legends.

Serum metabolite and HOMA-IR analysis

Blood samples were collected after 20 weeks of ND or HFD feeding or after 6, 24, and 48 hours of fasting and 24 hours of refeeding for the fasting/refeeding experiment. Cholesterol (LabAssay Cholesterol, Wako) and TG (Triglycerides Kit, Sigma) concentrations in serum were determined according to the manufacturers' protocols. Serum insulin levels were quantified either by using a magnetic bead based immunoassay kit (Bio-Plex Pro mouse insulin, Bio-Rad) and MAGPIX multiplex reader (Bio-Rad) or by the mouse insulin ELISA Kit (Crystal Chem) and a SPARK plate reader (Tecan) according to the manufacturers' guidelines. HOMA-IR was calculated with the following formula: fasting insulin (mU/ml) × fasting glucose (mg/dl) divided by 405 using blood from mice that were fasted overnight.

VLDL secretion

Mice were fasted overnight before they received a retro-orbital injection of 0.5 mg/g BW tyloxapol. Blood was collected at the 0-, 1-, 2-, 4-, and 6-hour time points and used for serum TG analysis as described above.

Metabolic measurements

Metabolic parameters such as energy expenditure, food intake, activity, and respiratory exchange ratio were determined in the PhenoMaster (TSE Systems) system as described before (*34*) after 23 weeks on specific diets.

Histological, immunohistochemistry, and immunofluorescence analyses

For histology, liver tissues were fixed in 10% formalin and embedded in paraffin. H&E or Sirius red staining of 2- to 4-μm liver sections was performed according to standard laboratory procedures. For immunohistochemistry, Ki-67 (H2, 95°C), cleaved caspase-3 (H2), B220 (H2), CD3 (H2, 95°C), F4/80 (E1), and collagen type IV (E1) antibodies were used with EDTA pretreatment (H2) or an enzyme pretreatment kit (E1) (Leica), respectively. For TUNEL staining, a fluorescence in situ cell death detection kit (Roche) was used according to the manufacturer's instructions.

Lipid extraction and TLC

Lipids were extracted according to the protocol of Bligh and Dyer with modifications (*35*). Briefly, 0.5 volumes of liver homogenate [1:100 in phosphate-buffered saline (PBS)] were acidified with 0.3 volumes of 0.2 N HCl. Subsequently, 3 volumes of MeOH/$CHCl_3$ (2:1, v/v), 1 volume of $CHCl_3$, and 1 volume of H_2O were added and mixed vigorously stepwise. The phases were separated by centrifugation, and the lower phase was transferred to a new tube and evaporated under a stream of nitrogen. The lipids were either resuspended in DMSO/H_2O for enzymatic quantification of TG and cholesterol (as described before) or in MeOH/$CHCl_3$ (1:1, v/v) for separation by TLC on a silica gel 60 plate (Merck) in the solvent mixtures of $CHCl_3$/MeOH/20% acetic acid (65:25:5, v/v/v), hexane/ethyl acetate/acetic acid (59:10:1, v/v/v), and pure hexane. Cholesteryl palmitate (for CE), triolein (for TG), oleic acid (for FFA), cholesterol (for FC), phosphatidylethanolamine (for PE), and phosphatidylcholine (for PL) were used as standards for the TLC. Lipid spots were visualized by dipping the plate in a hydrous solution of 2.5% 12-molybdophosphoric acid (Alfa Aesar), cerium (IV) sulfate (Sigma), and 6% H_2SO_4 and heating at 200°C until the bands appear. Densitometric analysis was performed using ImageJ and known concentrations of the standards.

Primary hepatocyte isolation and culture

Primary mouse hepatocytes were prepared by the collagen perfusion method. Eight- to 12-week-old male mice were anesthetized with ketamine/xylazine, and the vena cava was cannulated. The portal vein was cut immediately, and the liver was perfused with Earle's balanced salt solution (without Ca^{2+}/Mg^{2+}; Thermo Fisher Scientific) supplemented with 0.5 mM EGTA. Subsequently, the buffer was replaced to Hanks' balanced salt solution with Ca^{2+}/Mg^{2+} (Biochrom) containing type I collagenase (100 U/ml) (Worthington). After sufficient digestion, the liver was excised and the gall bladder was removed. Cells were liberated into Dulbecco's modified Eagle's medium (DMEM) supplemented with 10% fetal bovine serum and 1% penicillin/streptomycin (P/S), filtered through a 100-μm cell strainer, and centrifuged (50*g*, 3 min, 4°C). Afterward, Percoll (GE Healthcare) mixed with respective amounts of 10× PBS and culture medium was used to form a gradient that allowed enrichment of the hepatocyte fraction (50*g*, 10 min, 4°C), which was washed three times with culture medium (50*g*, 3 min, 4°C). Hepatocytes were then plated on collagen type I–coated 6- or 12-well plates (BD). After 4 to 6 hours, to allow attachment, the medium was replaced by fasting medium [DMEM supplemented with 0.2% FFA-free BSA (Sigma) and 1× P/S], and the cells were used the following day unless otherwise noted. For PKD3 phosphorylation studies, primary hepatocytes were incubated either with 1,2-dioctanoyl-*sn*-glycerol (Enzo Life Sciences) for 4, 6, and 8 hours or with oleic acid bound to albumin (Sigma) for 4 and 20 hours.

Adenovirus infection

Primary hepatocytes were infected 4 to 6 hours after plating with adenoviruses expressing either enhanced green fluorescent protein (EGFP) (Ad-EGFP) or a constitutively active form of PKD3 (Ad-mycPKD3ca) at an multiplicity of infection (MOI) of 10. Medium was replaced the following morning, and cells were used for experiments 36 to 48 hours after infection. Transduction efficiency, which was 100%, was assessed by analyzing the expression of the EGFP reporter (which was present in all adenoviruses).

Small interfering RNA transfections

Primary hepatocytes were transfected 4 to 6 hours after plating with *siNonTargeting* (60 nM), *siSrebp1* (30 nM), or *siSrebp2* (30 nM) (Dharmacon) using the Lipofectamine RNAiMAX transfection reagent (Invitrogen) according to the manufacturers' recommendations. Medium was replaced the following morning, and cells were used for experiments 36 to 48 hours after infection.

Lipogenesis assay

De novo lipogenesis assay was performed 1 day after the isolation of primary hepatocytes. Cells were incubated with a lipogenic medium (DMEM with 25 mM glucose, 0.2% FFA-free BSA, and 1× P/S) supplemented with 0.5 mM sodium acetate and ^{3}H-acetate (4 μCi/ml) (PerkinElmer) at basal or insulin (100 nM)–stimulated conditions for 4 to 6 hours. Cells were then washed twice with PBS and scraped into 0.1 N HCl. Subsequently, the lipids were extracted similarly as described before. Homogenate (0.8 volume) was mixed stepwise with 3 volumes of MeOH/$CHCl_3$ (2:1, v/v), 1 volume of $CHCl_3$, and 1 volume of H_2O. The phases were separated by centrifugation (3000*g*, 10 min), and the lower phase was transferred to a new tube, which was washed once with upper-phase MeOH/$CHCl_3$/H_2O (15:175:180, v/v/v) (3000*g*, 10 min). Last, the lower phase was transferred to a scintillation tube and evaporated under a stream of nitrogen. The dried lipids were resuspended in 4 ml of scintillation liquid before lipid scintillation counting. The lipogenesis rate was calculated as the amount of tritium incorporated into the newly formed lipids (measured in dpm) per total protein (Bradford, Bio-Rad) per hour. Alternatively, the extracted lipids were separated on a TLC plate as described before. The stained lipid spots were scraped and analyzed by lipid scintillation counting. To measure de novo lipogenesis in vivo, mice were fed an HFD for 8 weeks. After overnight fasting, mice were refed with an HFD for 4 hours before they received an intraperitoneal dose of 8 mCi [^{3}H]-water/100 g BW. After 2 hours, the livers were excised, and liver pieces (three per mouse) were homogenized 1:5 in 0.1 N HCl, followed by lipid extraction as described above. For inhibitor treatments, 10 μM Akti-1/2, 0.7 μM KU0063794, and 0.7 μM rapamycin were

added 4 to 6 hours after plating and 16 hours before the experiment, whereas 1 μM CRT0066101 was added 1 hour before the experiment.

FA oxidation

Hepatocytes were serum fasted overnight and incubated with DMEM containing ^{3}H-oleic acid (2 μCi/ml) (PerkinElmer) and 0.2 mM oleic acid bound to BSA (Sigma) at basal or insulin (100 nM)–stimulated conditions for 3 hours. Subsequently, the supernatant was collected, and the cells were washed twice with PBS and scraped in 0.1 N HCl to determine the protein concentration. Then, 1 volume of MeOH/$CHCl_3$ (2:1, v/v) and 1 volume of 2 M KCl/2 M HCl (1:1, v/v) were added to 0.5 volume of the supernatant and mixed stepwise. The phases were separated by centrifugation (3000*g*, 10 min), and the upper phase was transferred to a new tube and the procedure was repeated once more. Last, the upper phase was transferred to a scintillation tube, and 4 ml of scintillation liquid was used for scintillation counting. The FA oxidation rate was calculated as the amount of tritium incorporated into ^3H_2O (measured in dpm) per total protein (Bradford, Bio-Rad) per hour.

Immunoblotting

Western blot was performed according to standard procedures. Briefly, 20 μg of protein lysates was separated by a 10% SDS–polyacrylamide gel electrophoresis and transferred on a polyvinylidene difluoride (PVDF) membrane and then probed overnight with corresponding primary antibodies (table S1). After incubation with corresponding mouse or rabbit horseradish peroxidase–conjugated secondary antibody, proteins were visualized using ECL Reagent in combination with x-ray films (Fuji) or with the Amersham Imager 600 (GE Healthcare) for densitometric analysis.

Real-time quantitative polymerase chain reaction analysis

Total RNA was extracted from tissue or cells using QIAzol Reagent (Qiagen) according to the manufacturer's instructions. Reverse transcription of 1 μg of RNA was performed by using the First Strand cDNA Synthesis Kit (Thermo Fisher Scientific). Real-time quantitative polymerase chain reaction (QPCR) was performed using PowerUp SYBR Green Master Mix (Thermo Fisher Scientific) on a QuantStudio 5 Real-Time PCR System (Thermo Fisher Scientific). Relative amounts of all mRNAs were calculated using the comparative C_T method normalized to the reference gene *Rpl13a*, *36B4*, or *Hprt1*. The primer sequences (sense and antisense) for mouse are listed in table S2. Absolute quantification of PKD isoform copy numbers in the liver was performed according to the standard protocol of Applied Biosystems. Briefly, the primers were designed to be located within same exons (table S2), and genomic DNA of known concentration was used to create a standard curve reflecting copy numbers.

Statistical analysis

Data are presented as mean values ± SEM. Significances were determined by using two-tailed Student's *t* test for independent groups or by using one-way analysis of variance (ANOVA), followed by the post hoc Tukey's test for multiple comparisons. *P* values of 0.05 or lower were considered as statistically significant.

SUPPLEMENTARY MATERIALS

stke.sciencemag.org/cgi/content/full/12/593/eaav9150/DC1

Fig. S1. Stimulation of hepatocytes with DAG suppresses expression of lipogenic genes.
Fig. S2. PKD3 deletion is restricted to the liver.
Fig. S3. Liver-specific PKD3 deletion does not affect metabolism of mice fed an ND.
Fig. S4. PKD3 does not affect proliferation, immune cell infiltration, or apoptosis in the liver.
Fig. S5. TG accumulation in the livers of $PKD3^{liver\Delta/\Delta}$ mice does not depend on FA oxidation or VLDL secretion.
Fig. S6. The abundance and/or phosphorylation of mTORC1/2 components are not affected by deletion or overexpression of PKD3 in hepatocytes.
Fig. S7. Quantifications of Western blots of control and PKD3-deficient primary hepatocytes.
Fig. S8. Quantifications of Western blots of EGFP- and PKD3ca-transduced primary hepatocytes.
Fig. S9. Liver-specific expression of PKD3ca improves glucose tolerance and insulin sensitivity.
Table S1. List of antibodies used for Western blotting and immunohistochemistry.
Table S2. Sequence of primers used for QPCR and genotyping.

REFERENCES AND NOTES

1. D. A. Fruman, H. Chiu, B. D. Hopkins, S. Bagrodia, L. C. Cantley, R. T. Abraham, The PI3K pathway in human disease. *Cell* **170**, 605–635 (2017).
2. V. T. Samuel, G. I. Shulman, Nonalcoholic fatty liver disease as a nexus of metabolic and hepatic diseases. *Cell Metab.* **27**, 22–41 (2018).
3. J. R. Krycer, L. J. Sharpe, W. Luu, A. J. Brown, The Akt–SREBP nexus: cell signaling meets lipid metabolism. *Trends Endocrinol. Metab.* **21**, 268–276 (2010).
4. S. J. H. Ricoult, B. D. Manning, The multifaceted role of mTORC1 in the control of lipid metabolism. *EMBO Rep.* **14**, 242–251 (2013).
5. V. T. Samuel, G. I. Shulman, Mechanisms for insulin resistance: Common threads and missing links. *Cell* **148**, 852–871 (2012).
6. M. C. Petersen, A. K. Madiraju, B. M. Gassaway, M. Marcel, A. R. Nasiri, G. Butrico, M. J. Marcucci, D. Zhang, A. Abulizi, X.-M. Zhang, W. Philbrick, S. R. Hubbard, M. J. Jurczak, V. T. Samuel, J. Rinehart, G. I. Shulman, Insulin receptor Thr 1160 phosphorylation mediates lipid-induced hepatic insulin resistance. *J. Clin. Invest.* **126**, 4361–4371 (2016).
7. V. T. Samuel, Z.-X. Liu, A. Wang, S. A. Beddow, J. G. Geisler, M. Kahn, X.-m. Zhang, B. P. Monia, S. Bhanot, G. I. Shulman, Inhibition of protein kinase Cε prevents hepatic insulin resistance in nonalcoholic fatty liver disease. *J. Clin. Invest.* **117**, 739–745 (2007).
8. E. Rozengurt, Protein kinase D signaling: Multiple biological functions in health and disease. *Physiology* **26**, 23–33 (2011).
9. A. Kleger, C. Loebnitz, G. V. Pusapati, M. Armacki, M. Müller, S. Tümpel, A. Illing, D. Hartmann, C. Brunner, S. Liebau, K. L. Rudolph, G. Adler, T. Seufferlein, Protein kinase D2 is an essential regulator of murine myoblast differentiation. *PLOS ONE* **6**, e14599 (2011).
10. T. S. Steiner, S. M. Ivison, Y. Yao, A. Kifayet, Protein kinase D1 and D2 are involved in chemokine release induced by toll-like receptors 2, 4, and 5. *Cell. Immunol.* **264**, 135–142 (2010).
11. O. Konopatskaya, S. A. Matthews, M. T. Harper, K. Gilio, J. M. E. M. Cosemans, C. M. Williams, M. N. Navarro, D. A. Carter, J. W. M. Heemskerk, M. Leitges, D. Cantrell, A. W. Poole, Protein kinase C mediates platelet secretion and thrombus formation through protein kinase D2. *Blood* **118**, 416–424 (2011).
12. J. Fielitz, M.-S. Kim, J. M. Shelton, X. Qi, J. A. Hill, J. A. Richardson, R. Bassel-Duby, E. N. Olson, Requirement of protein kinase D1 for pathological cardiac remodeling. *Proc. Natl. Acad. Sci. U.S.A.* **105**, 3059–3063 (2008).
13. M.-S. Kim, J. Fielitz, J. McAnally, J. M. Shelton, D. D. Lemon, T. A. McKinsey, J. A. Richardson, R. Bassel-Duby, E. N. Olson, Protein kinase D1 stimulates MEF2 activity in skeletal muscle and enhances muscle performance. *Mol. Cell. Biol.* **28**, 3600–3609 (2008).
14. C. Li, J. Li, X. Cai, H. Sun, J. Jiao, T. Bai, X. W. Zhou, X. Chen, D. L. Gill, X. D. Tang, Protein kinase D3 is a pivotal activator of pathological cardiac hypertrophy by selectively increasing the expression of hypertrophic transcription factors. *J. Biol. Chem.* **286**, 40782–40791 (2011).
15. S. A. Matthews, P. Liu, M. Spitaler, E. N. Olson, T. A. McKinsey, D. A. Cantrell, A. M. Scharenberg, Essential role for protein kinase D family kinases in the regulation of class II histone deacetylases in B lymphocytes. *Mol. Cell. Biol.* **26**, 1569–1577 (2006).
16. A. Ittner, H. Block, C. A. Reichel, M. Varjosalo, H. Gehart, G. Sumara, M. Gstaiger, F. Krombach, A. Zarbock, R. Ricci, Regulation of PTEN activity by p38δ-PKD1 signaling in neutrophils confers inflammatory responses in the lung. *J. Exp. Med.* **209**, 2229–2246 (2012).
17. M. Ferdaoussi, V. Bergeron, B. Zarrouki, J. Kolic, J. Cantley, J. Fielitz, E. N. Olson, M. Prentki, T. Biden, P. E. MacDonald, V. Poitout, G protein-coupled receptor (GPR)40-dependent potentiation of insulin secretion in mouse islets is mediated by protein kinase D1. *Diabetologia* **55**, 2682–2692 (2012).
18. G. Sumara, I. Formentini, S. Collins, I. Sumara, R. Windak, B. Bodenmiller, R. Ramracheya, D. Caille, H. Jiang, K. A. Platt, P. Meda, R. Aebersold, P. Rorsman, R. Ricci, Regulation of PKD by the MAPK p38δ in insulin secretion and glucose homeostasis. *Cell* **136**, 235–248 (2009).

19. M. C. Löffler, A. E. Mayer, J. T. Viera, A. L. Valdes, R. El-Merahbi, C. P. Ade, T. Karwen, W. Schmitz, A. Slotta, M. Erk, S. Janaki-Raman, N. Matesanz, J. L. Torres, M. Marcos, G. Sabio, M. Eilers, A. Schulze, G. Sumara, Protein kinase D1 deletion in adipocytes enhances energy dissipation and protects against adiposity. *EMBO J.* **37**, e99182 (2018).
20. T. Zhang, U. Braun, M. Leitges, PKD3 deficiency causes alterations in microtubule dynamics during the cell cycle. *Cell Cycle* **15**, 1844–1854 (2016).
21. C. Postic, M. Shiota, K. D. Niswender, T. L. Jetton, Y. Chen, J. M. Moates, K. D. Shelton, J. Lindner, A. D. Cherrington, M. A. Magnuson, Dual roles for glucokinase in glucose homeostasis as determined by liver and pancreatic β cell-specific gene knock-outs using Cre recombinase. *J. Biol. Chem.* **274**, 305–315 (1999).
22. A. Suzuki, A. M. Diehl, Nonalcoholic steatohepatitis. *Annu. Rev. Med.* **68**, 85–98 (2017).
23. H. Ono, H. Shimano, H. Katagiri, N. Yahagi, H. Sakoda, Y. Onishi, M. Anai, T. Ogihara, M. Fujishiro, A. Y. I. Viana, Y. Fukushima, M. Abe, N. Shojima, M. Kikuchi, N. Yamada, Y. Oka, T. Asano, Hepatic akt activation induces marked hypoglycemia, hepatomegaly, and hypertriglyceridemia with sterol regulatory element binding protein involvement. *Diabetes* **52**, 2905–2913 (2003).
24. M. Fleischmann, P. B. Iynedjian, Regulation of sterol regulatory-element binding protein 1 gene expression in liver: Role of insulin and protein kinase B/cAkt. *Biochem. J.* **349**, 13–17 (2000).
25. K. F. Leavens, R. M. Easton, G. I. Shulman, S. F. Previs, M. J. Birnbaum, Akt2 is required for hepatic lipid accumulation in models of insulin resistance. *Cell Metab.* **10**, 405–418 (2009).
26. N. Ozgen, M. Obreztchikova, J. Guo, H. Elouardighi, G. W. Dorn II, B. A. Wilson, S. F. Steinberg, Protein kinase D links Gq-coupled receptors to cAMP response element-binding protein (CREB)-Ser133 phosphorylation in the heart. *J. Biol. Chem.* **283**, 17009–17019 (2008).
27. A. Hagiwara, M. Cornu, N. Cybulski, P. Polak, C. Betz, F. Trapani, L. Terracciano, M. H. Heim, M. A. Rüegg, M. N. Hall, Hepatic mTORC2 activates glycolysis and lipogenesis through Akt, glucokinase, and SREBP1c. *Cell Metab.* **15**, 725–738 (2012).
28. J. L. Yecies, H. H. Zhang, S. Menon, S. Liu, D. Yecies, A. I. Lipovsky, C. Gorgun, D. J. Kwiatkowski, G. S. Hotamisligil, C.-H. Lee, B. D. Manning, Akt stimulates hepatic SREBP1c and lipogenesis through parallel mTORC1-dependent and independent pathways. *Cell Metab.* **14**, 21–32 (2011).
29. T. Porstmann, C. R. Santos, B. Griffiths, M. Cully, M. Wu, S. Leevers, J. R. Griffiths, Y.-L. Chung, A. Schulze, SREBP activity is regulated by mTORC1 and contributes to Akt-dependent cell growth. *Cell Metab.* **8**, 224–236 (2008).
30. K. Cai, R. El-Merahbi, M. Loeffler, A. E. Mayer, G. Sumara, Ndrg1 promotes adipocyte differentiation and sustains their function. *Sci. Rep.* **7**, 7191 (2017).
31. Y. Wang, J. Viscarra, S.-J. Kim, H. S. Sul, Transcriptional regulation of hepatic lipogenesis. *Nat. Rev. Mol. Cell Biol.* **16**, 678–689 (2015).
32. B. Stiles, Y. Wang, A. Stahl, S. Bassilian, W. P. Lee, Y.-J. Kim, R. Sherwin, S. Devaskar, R. Lesche, M. A. Magnuson, H. Wu, Liver-specific deletion of negative regulator Pten results in fatty liver and insulin hypersensitivity. *Proc. Natl. Acad. Sci. U.S.A.* **101**, 2082–2087 (2004).
33. Y. Izawa, M. Yoshizumi, Y. Fujita, N. Ali, Y. Kanematsu, K. Ishizawa, K. Tsuchiya, T. Obata, Y. Ebina, S. Tomita, T. Tamaki, ERK1/2 activation by angiotensin II inhibits insulin-induced glucose uptake in vascular smooth muscle cells. *Exp. Cell Res.* **308**, 291–299 (2005).
34. J. Trujillo Viera, R. El-Merahbi, B. Nieswandt, D. Stegner, G. Sumara, Phospholipases D1 and D2 suppress appetite and protect against overweight. *PLOS ONE* **11**, e0157607 (2016).
35. E. G. Bligh, W. J. Dyer, A rapid method of total lipid extraction and purification. *Can. J. Biochem. Physiol.* **37**, 911–917 (1959).

Acknowledgments: We thank O. Sumara for the critical comments to our manuscript, A. Schürmann and C. Baumeister for introducing us to primary hepatocyte isolation, J. Hetzer and D. Heide for performing the immunohistochemical stainings, and K. Aurbach, I. Becker, and D. Cherpokova for experimental assistance. **Funding:** This project was supported by the EFSD/Janssen Rising Star Fellowship Programme (2013) from the European Foundation for the Study of Diabetes and by the Starting Grant (SicMetabol) from the European Research Council (ERC) and internal funds of the Rudolf Virchow Center for Experimental Biomedicine. R.E.-M. and G.S. were also funded by the Emmy Noether grant from the German Research Foundation (no. Su 820/1-1). M.H. was supported by an ERC Consolidator grant (HepatoMetaboPath). A.S. was supported by a German Research Foundation grant (FOR2314, SCHU2670/1-1). **Author contributions:** A.E.M. and G.S. conceived the study, designed the experimental procedures, and wrote the manuscript. A.E.M. performed the majority of the experimental work and analyzed the data. M.C.L., A.E.L.V., R.E.-M., J.T.V., and M.E. performed parts of the experiments. W.S. participated in the experimental design and carried out the mass spectrometry. M.L., T.Z., and U.B. provided the *PKD3*$^{f/f}$ mice. M.H. and A.S. contributed to the experimental design. **Competing interests:** The authors declare that they have no competing interests. **Data and materials availability:** The *PKD3*$^{f/f}$ mice require a material transfer agreement by the PKC Research Consult (Cologne, Germany). All data needed to evaluate the conclusions in the paper are present in the paper or the Supplementary Materials.

Submitted 31 October 2018
Accepted 19 July 2019
Published 6 August 2019
10.1126/scisignal.aav9150

Citation: A. E. Mayer, M. C. Löffler, A. E. Loza Valdés, W. Schmitz, R. El-Merahbi, J. T. Viera, M. Erk, T. Zhang, U. Braun, M. Heikenwalder, M. Leitges, A. Schulze, G. Sumara, The kinase PKD3 provides negative feedback on cholesterol and triglyceride synthesis by suppressing insulin signaling. *Sci. Signal.* **12**, eaav9150 (2019).

Science Signaling

The kinase PKD3 provides negative feedback on cholesterol and triglyceride synthesis by suppressing insulin signaling

Alexander E. Mayer, Mona C. Löffler, Angel E. Loza Valdés, Werner Schmitz, Rabih El-Merahbi, Jonathan Trujillo Viera, Manuela Erk, Thianzhou Zhang, Ursula Braun, Mathias Heikenwalder, Michael Leitges, Almut Schulze and Grzegorz Sumara

Sci. Signal. **12** (593), eaav9150.
DOI: 10.1126/scisignal.aav9150

A limit for liver lipid overload

Hepatocytes respond to insulin by accumulating triglycerides and cholesterol. Excessive lipid accumulation in the liver can result in nonalcoholic fatty liver disease (NAFLD), the more severe forms of which are risk factors for the development of liver cirrhosis and cancer. Mayer *et al.* found that activation of PKD3 by insulin signaling served as a negative feedback mechanism to prevent hepatic lipid accumulation. Mice lacking PKD3 in the liver showed increased insulin signaling, triglyceride and cholesterol synthesis, and steatosis in response to a high-fat diet. In contrast, overexpression of a constitutively active form of PKD3 attenuated insulin signaling in the liver and resulted in insulin resistance. Thus, PKD3 activity curtails insulin signaling and, therefore, lipid synthesis and accumulation in the liver.

Science Signaling (ISSN 1937-9145) is published by the American Association for the Advancement of Science, 1200 New York Avenue NW, Washington, DC 20005. The title *Science Signaling* is a registered trademark of AAAS.